A Brief Report on

Iterative Design Process for the Pal-V Flying Vehicle Chassis with FEA

By

Daniel Yin and Zachary Yamaoka

Design Engineering MEng

Dyson School of Design Engineering

Imperial College London

1 Introduction

PAL-V is a completely new type of vehicle that is able to transform between helicopter and car. This enables it to drive at up to 160 km/h on a highway, and cruise at 140 km/h through the sky [1]. PAL-V markets it self as the worlds first flying car and expects to hand over keys to the first customers in 2019 [1]. A failure in one of PAL-V's first models would most likely mean the end of the Dutch company and 20 years of research. It is essential that the chassis is structurally sound and comfortable. For this purpose, a number of technical requirements have been specified. In addition to being light weight, the chassis must:

- Support a 7 kN landing force with a safety factor of 1.5
- Have an effective life of one billion rotations of the rotor blade
- Have a fundamental frequency larger than 50 Hz

To meet these requirements, a chassis was designed in the Solidworks CAD software (refer to Figure 1). The finite element method was then used to validate the structure.

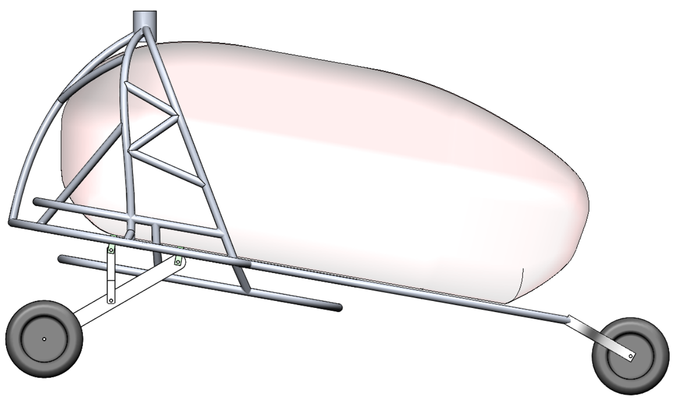

Figure 1. 3D model of the designed chassis

2 Methods

2.1 Design Methods

An iterative method, involving all four team members, was used to cover a large design space. Starting from a base model, at each stage, team members made a small modification to the chassis.

Key considerations which influenced the modifications included

- Considerations of direction of forces and the directions of sensitivity. For instance, the front to back moment will be harder to support than the left to right moment (refer to Section 2.3).
- Consideration of the location of forces. To prevent large deflections, the bearings, which transfer the landing force (refer to Section 2.3), should be supported as close as possible to point of applications.
- Consideration of stress distribution. Over constrained structures lead to stress concentrations.
- Consideration of structural connections. Triangles or cross braced squares are preferable.

FE Static and frequency studies were then run to evaluate the changes. To better interpret static results, the isoclipping tool was used to identify areas of high stress. Local mesh refining was then done in these areas of interest to improve resolution. After running the studies, the best design was selected and shared with team members for further iteration.

2.2 Modelling Assumptions

Before a problem can be solved through finite element analysis, it must first be modelled. While the essential features of the original problem are present in the model used for this analysis, a number of assumptions were made.

- It is assumed that bearing contact surfaces and rotor hub represent the mechanisms in sufficient detail. In reality such mechanical components would be more complex.

- It is assumed that extra structural components required to connected the designed external chassis to the restricted internal area are negligible

- It is assumed that the chassis will be made from 7075-T6 aluminum. Data for elastic modulus, yield strength, passion ratio, density and S-N curve of material is provided from the Solidworks library and taken to be accurate

- It is assumed that connecting the chassis structural members (tubes with 50mm outer diameter and 5mm thickness) through Solidworks body merging and filleting, sufficiently represents an actual welded joint

- It is assumed that deflection of the structure is small, such that linear analysis is sufficiently accurate.

- All loading cases are assumed to be static or quasi-static. In reality, inertial effects due to the acceleration of the helicopter would impact loading.

2.3 Loading Cases

Two loading cases were assessed:

1. As the vehicle lands, a 7 kN static load is applied to one side of the chassis. In simulation, it was assumed that this load was transferred through the damper and wheel arm support, to the bearings. The reaction forces at the bearings were calculated by formulating and solving 4 equations of motion (refer to Appendix B). The forces were found to be -14 kN and 7 kN for the back and front bearing respectively.

In simulation, these two static forces are applied to chassis in a direction vertical to the ground. Further, the forces are only distributed on either the top of the bottom of the bearing. It is believed that a single sided loading better represents how a physical bearing would transfer load.

2. During operation, centrifugal forces of the rotating blades apply a 2kNm moment to the inner surface of the rotor hub. Further, this load is cyclic and changes direction as the the helicopter blade spins.

In simulation, four separate studies were created for each direction of the moment. A torque was applied to the inner surface of the rotor hub and the direction was set by referencing an axis that ran through the center of the hub.

2.4 Boundary Conditions

1. In static studies for load case one, elements in the bearings opposite to the loaded wheel are fixed in all three degrees of freedom – translation in x, y, z

2. In static studies for load case two, the base of the chassis was fixed. Specifically, as seen in Figure 2, a fixed geometry constrained is applied to the surfaces in contact with the bearings and the front wheel. Identical boundaries are used for frequency studies.

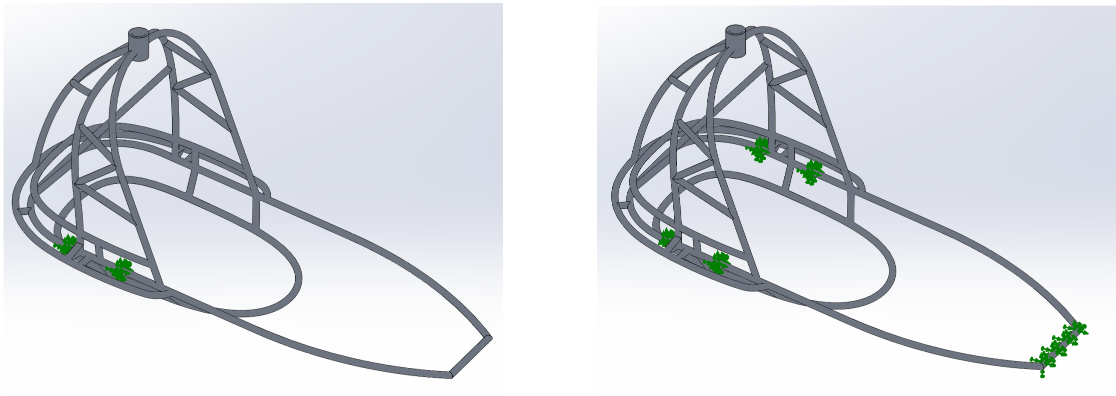

Figure 2. Boundary conditions for static studies. Fixtures on left used for Loading Case 1 and on the right for Loading Case 2.

2.5 Meshing

All three meshing algorithm in Solidworks were tested. Ultimately though, the majority of discretization was done using the blended curvature-based mesh. This algorithm more consistently discretized models when the standard and curvature based algorithm failed. Further settings included, using 4 Jacobian points, and a starting maximum element size of approximately 100 mm.

3 Results

3.1 Static

Presented below are a series of mesh convergence studies for the static loading cases. In each instance, a h-method was iteratively employed to achieve a better approximation of the real stress. This was accomplished by decreasing the maximum and minimum element size until the solution converged. Interestingly, simply refining mesh was not sufficient to reach convergence in all studies – reasons for which are discussed in Section 4.5.

Loading Case 1

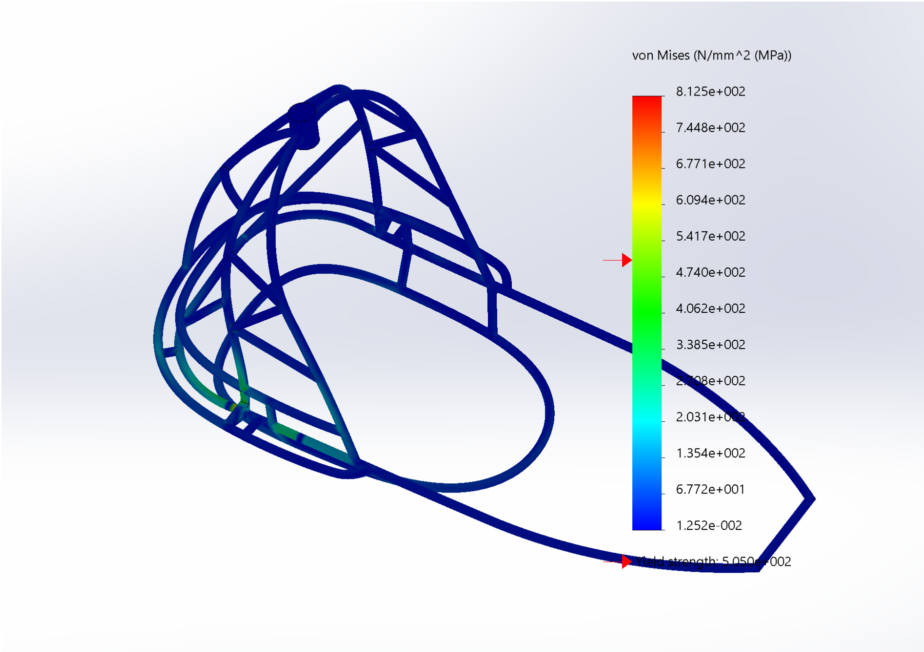

Figure 3. Stress visualization for +7 kN and -14 kN landing force applied to chassis. Maximum von Mises stress was 812 MPa.

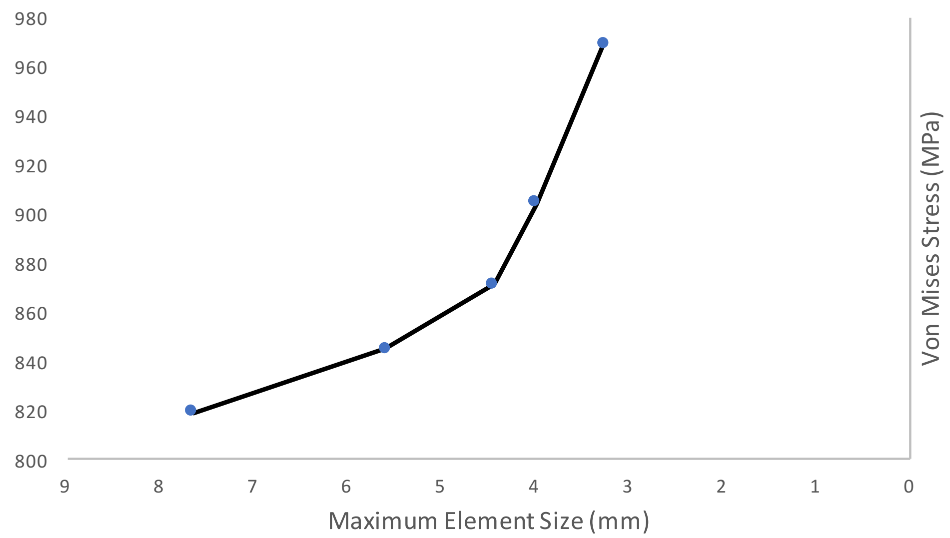

Figure 4. Mesh convergence plot for Loading Case 1. Stress increases at finer mesh sizes – indicates a stress singularity. Refer to Appendix B for data.

Loading Case 2: Direction 1

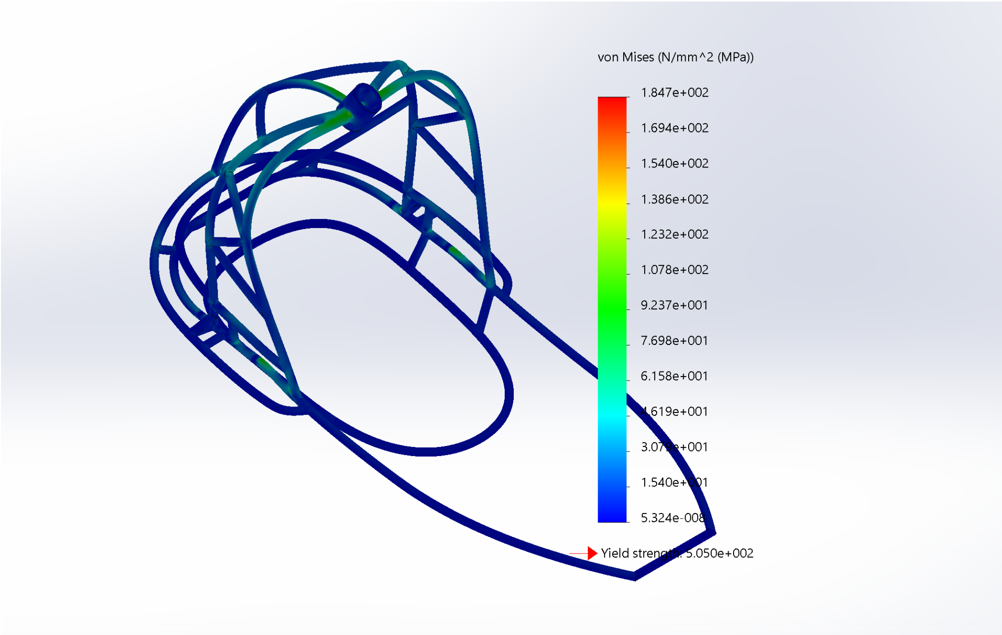

Figure 5. Stress visualization for 2 kN applied at rotor hub. Moment is applied around the left to right axis – in the back to front direction. Maximum von Mises stress was 184 MPa.

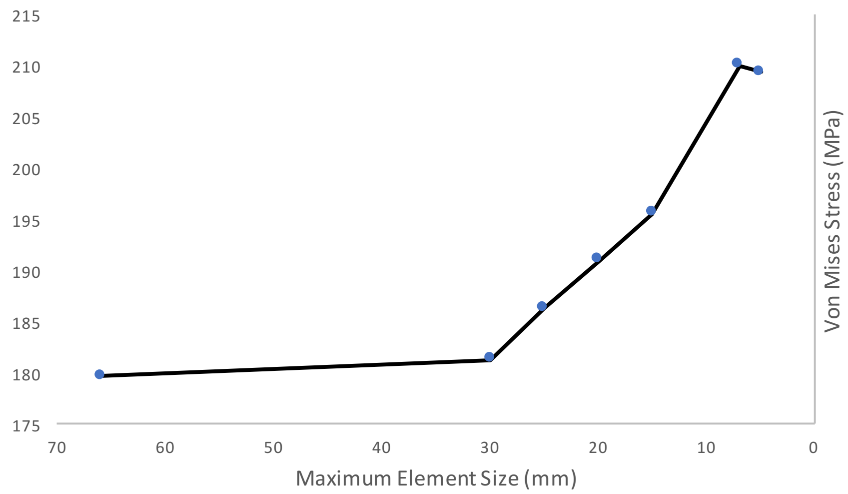

Figure 6. Mesh convergence plot for moment Direction 1. Maximal stress peak at 5mm max. element size. Indicated the a potential start of convergence. Refer to Appendix B for data.

Loading Case 2: Direction 2

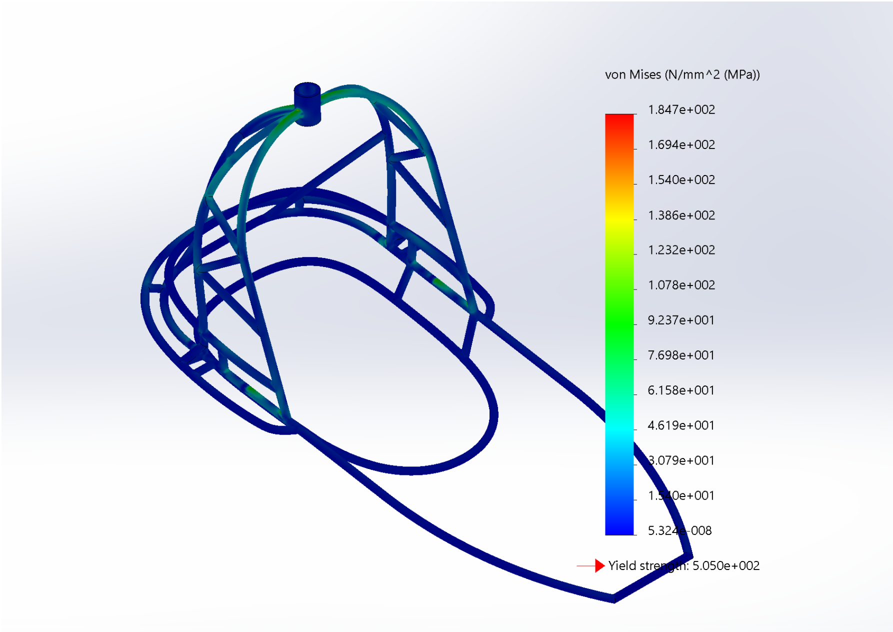

Figure 7. Stress visualization for 2 kN applied at rotor hub. Moment is applied around the left to right axis – in the front to back direction. Maximum von Mises stress was 187 MPa.

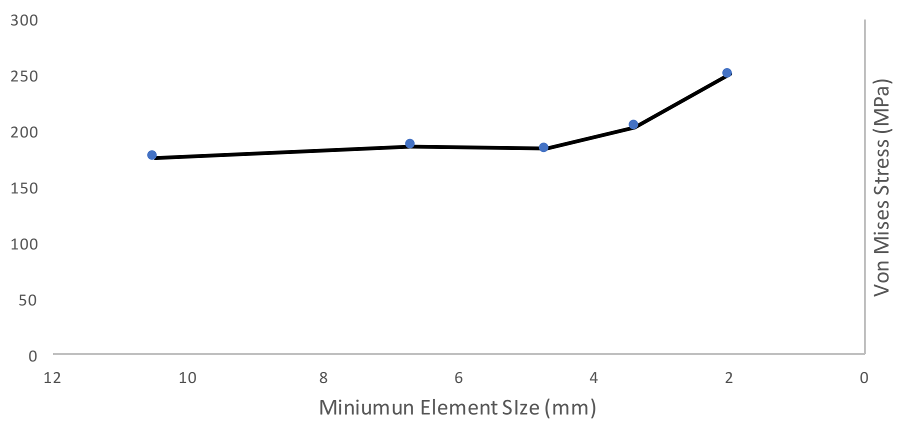

Figure 8. Mesh convergence plot for Loading Case 2: Direction 2. Refer to Appendix B for data.

Loading Case 2: Direction 3

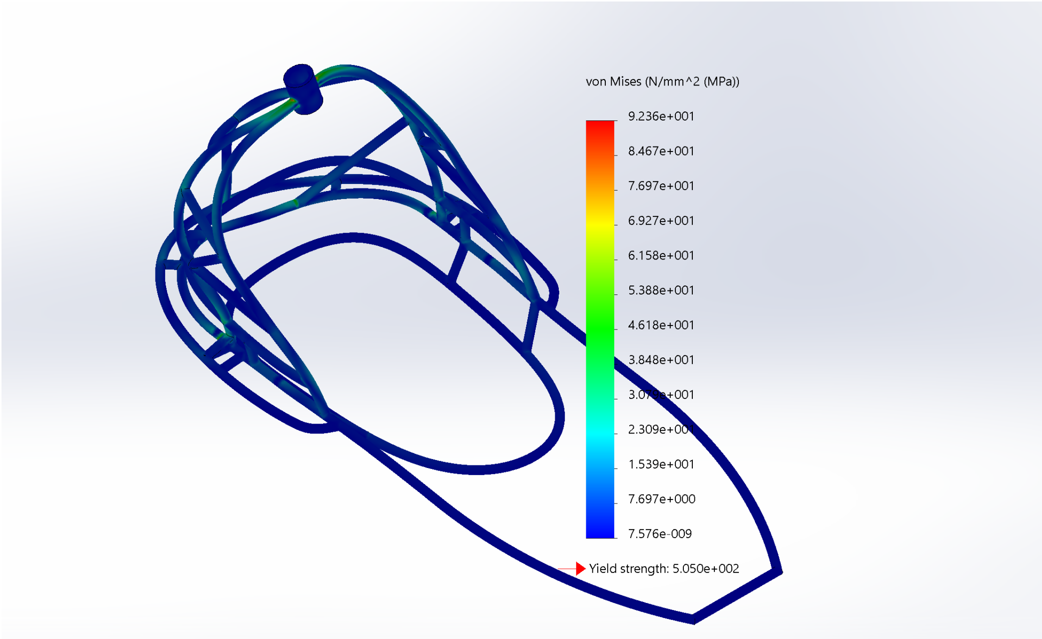

Figure 9. Stress visualization for 2 kN applied at rotor hub. Moment is applied around the back to front axis – in the left to right direction. Maximum von Mises stress was 92 MPa.

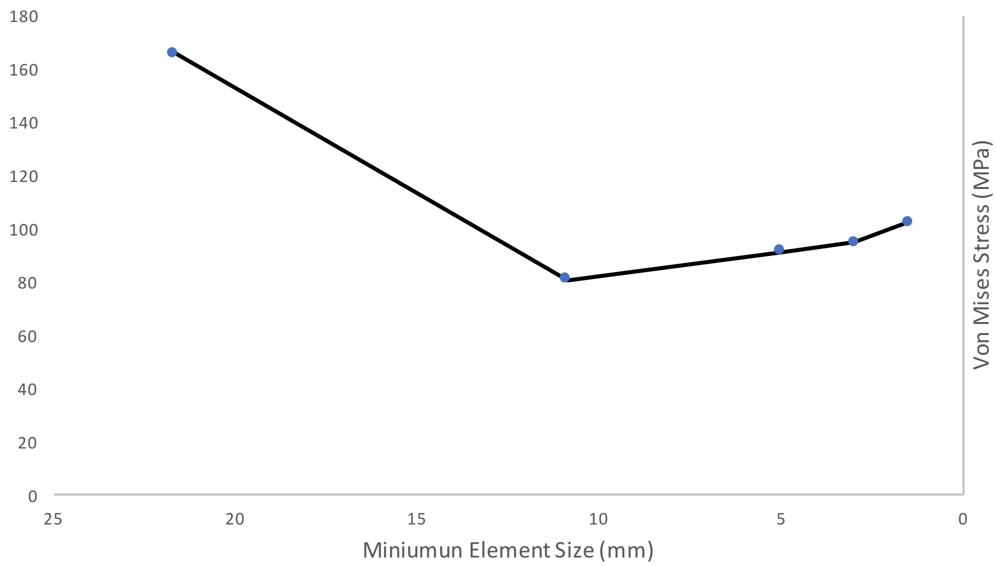

Figure 10. Mesh convergence plot for Loading Case 2: Direction 3. Refer to Appendix B for data.

Loading Case 2: Direction 4

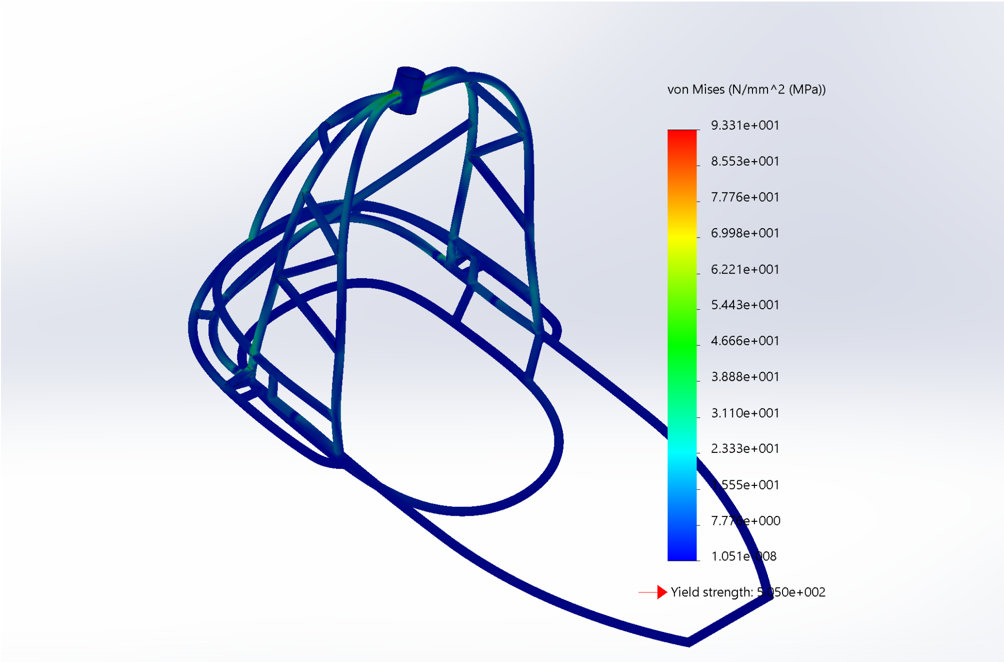

Figure 11. Stress visualization for 2 kN applied at rotor hub. Moment is applied around the back to front axis – in the right to left direction. Maximum von Mises stress was 93 MPa.

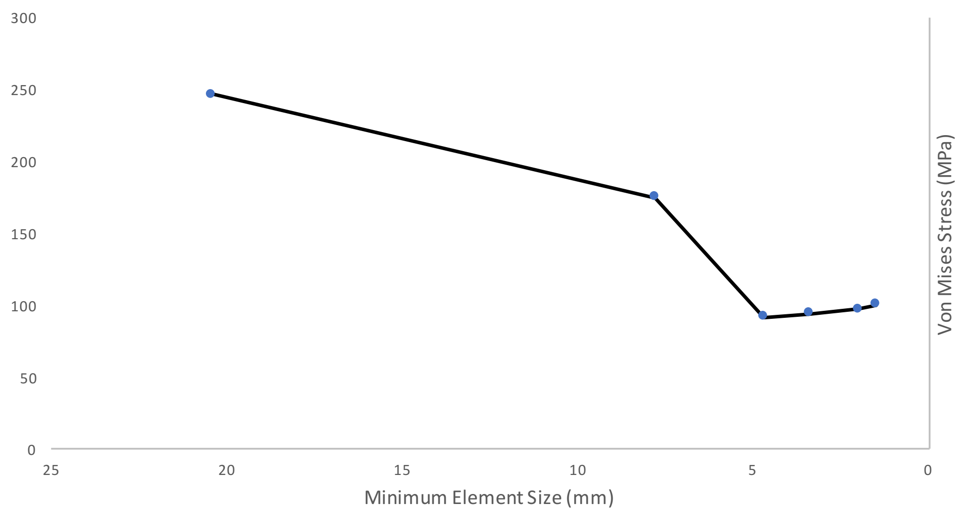

Figure 12. Mesh convergence plot for Loading Case 2: Direction 4. Refer to Appendix B for data.

3.2 Local Mesh Refinement

During static studies, areas of high stress were identified with the isocline tool and locally improved. This allowed accuracy in areas of high interest to improve at a lower computational cost.

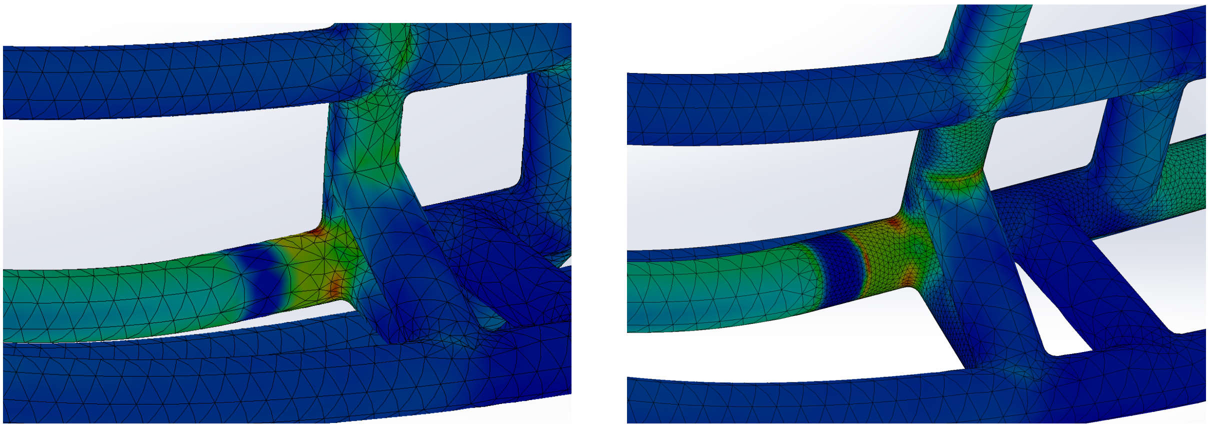

Figure 13. Mesh control on identified stress concentration area at the bottom of chassis.

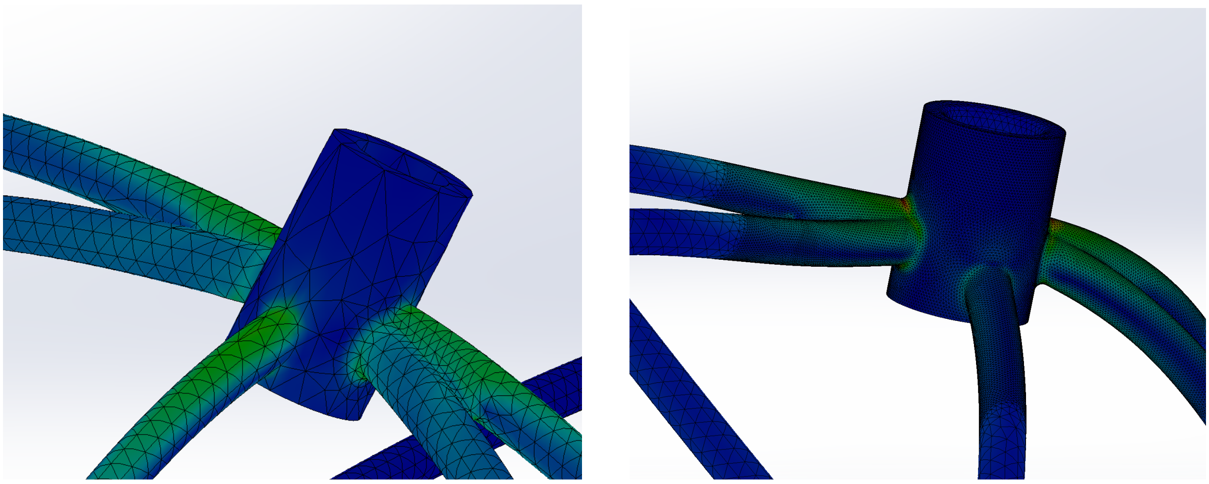

Figure 14. Mesh control on the outer surface of the rotor hub and the connected structures.

3.3 Fatigue

Fatigue studies were ran using all four directions of the cyclic loading case. In addition to the specified aluminum alloy (7075-T6), magnesium alloy was also tested. For magnesium alloy, the fatigue SN curve was derived based on ASME carbon steel curves.

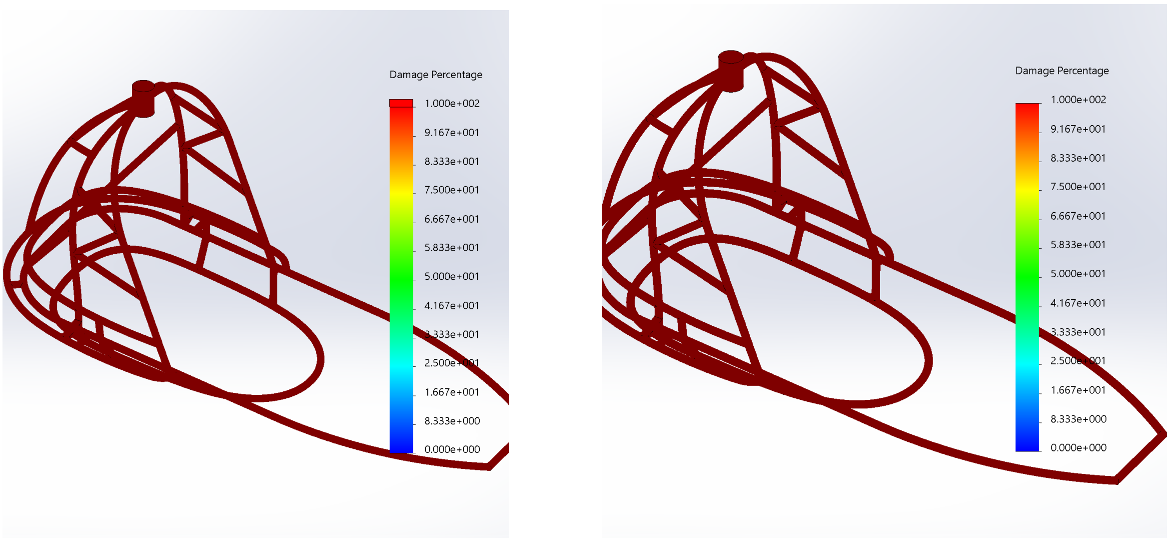

Figure 15. Damage given 1B cycles lifetime – aluminum on the left and magnesium is on the right. Values are capped at 100% damage.

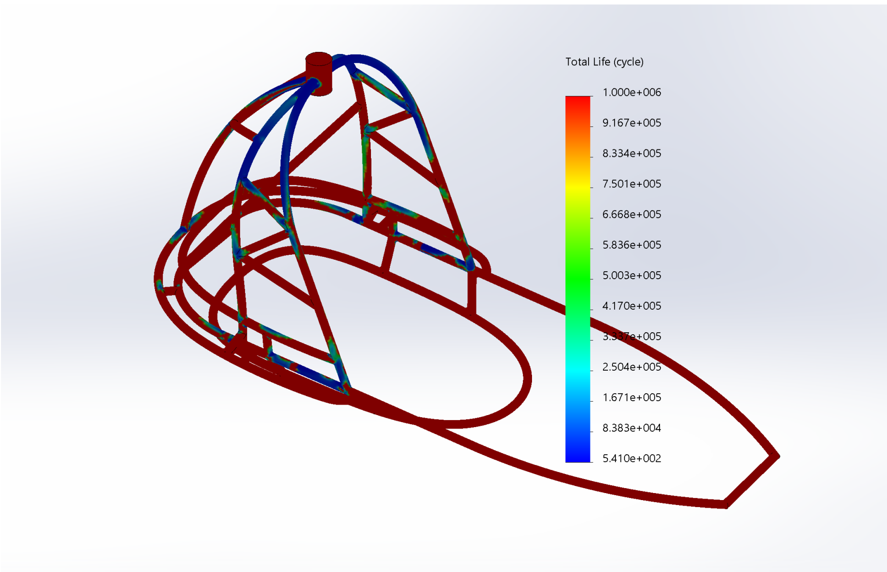

Figure 16. Expected cycles for the magnesium alloy chassis. As expected, areas of higher stress have a lower expected total life.

3.4 Frequency

Vibration studies were conducted to determine the fundamental frequency of the proposed chassis. The visualizations below, show the first mode shape for a number of the models proposed while iterating to increase fundamental frequency.

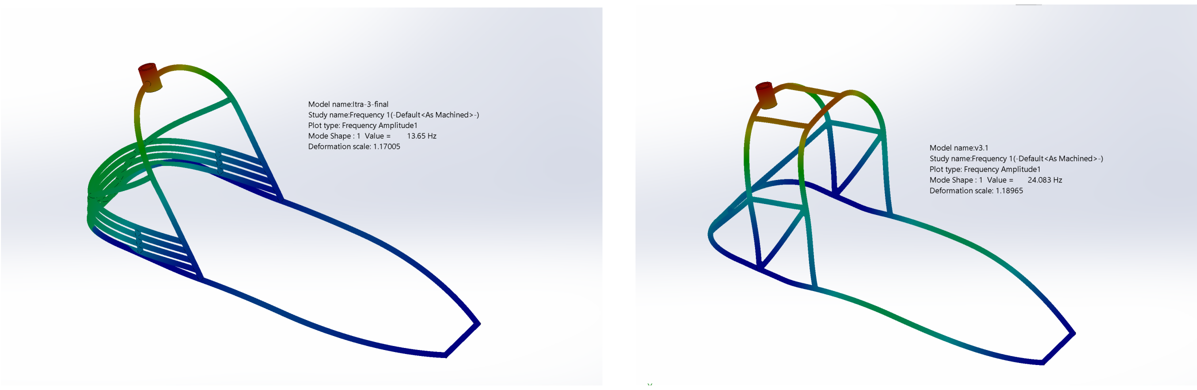

Figure 17. Mode shape for two earlier iterations. Fundamental frequencies were calculated as 13.6 Hz and 24.6 Hz respectively.

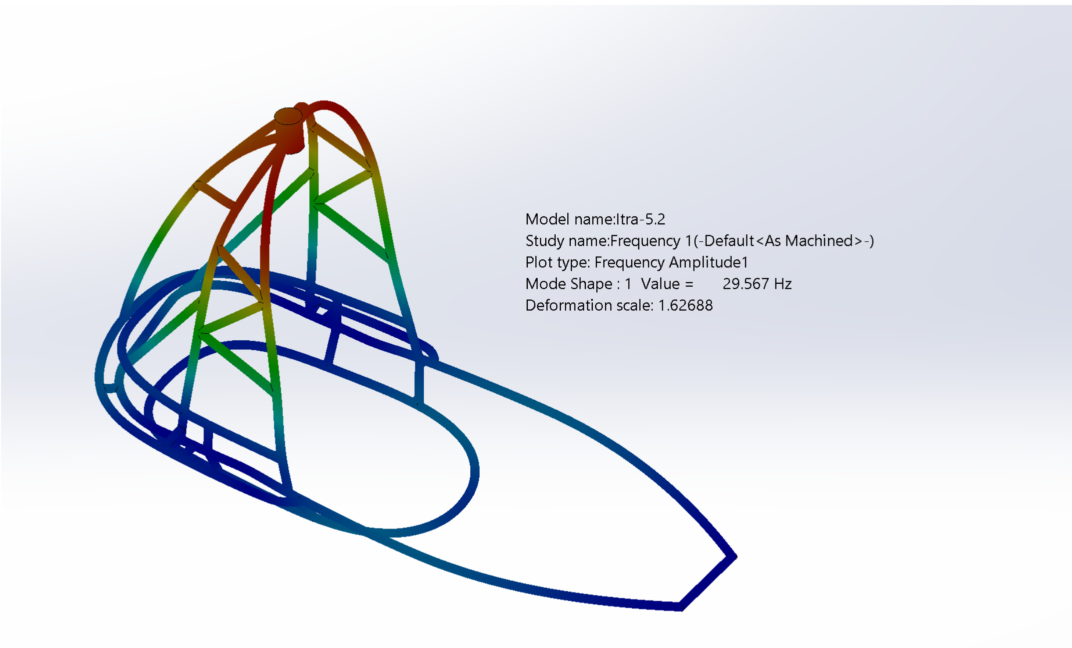

Figure 18. First mode shape for final chassis. Associated fundamental frequency was calculated as 29.567 Hz.

3.5 Sanity Checks

Preliminary Analysis

Prior to beginning FEA analysis, first order calculations were done. The intent was to determine an upper bound to the expected stress magnitudes.

Stress of 7 kN force applied directly and normal to structural member:

$$\sigma = \frac{F}{A} \qquad A_{\textbf{tube}} = \pi(r^2_{\textbf{outer}} - r^2_{\textbf{inner}}) \qquad \sigma = \frac{7000}{1.4\textbf{e-}3} = 4.6 \textbf{ MPa}$$

Stress due to direct 2 kNm moment:

$$\sigma_x = \frac{My}{I} \qquad I_{\textbf{tube}} = \frac{\pi}{2}(r^4_{\textbf{outer}} - r^4_{\textbf{inner}}) \qquad \sigma_x = \frac{2000 \times 0.05}{1.6\textbf{e-6}} = 59.2 \textbf{ MPa}$$

Stress due to 7 kN force applied at 1.5 m distance. This modelled the bearings being connected by a single beam:

$$\sigma_x = \frac{10500 \times 0.05}{1.6\textbf{e-6}} = 322 \textbf{ MPa}$$

Maximum expected stress:

$$\sigma_x = \frac{My}{I} + \frac{F}{A} \qquad \sigma_{max} = 326.6 \textbf{ MPa}$$

The calculated stress under estimated the maximal FEA result. This likely occurred because no consideration was given to stress concentrations. However, using a probe tool to test a value near a stress concentration in the model, the calculated theoretical stress is certainly within the right magnitude. Thus indication is given, that the conducted FEA studies may be correct.

Reaction Forces

By newtons second law, in a static study:

$$\sum F_{x,y,z} = 0$$

Thus reactions forces can be monitored to ensure that the model is behaving as expected and applied loads are correct. In a particular iteration of the chassis, a study for Loading Case 1 indicated a 3x increase in stress after just a small modification to the structure. Upon checking the reaction forces, it was realized that 21 kN instead of 7 kN had been applied.

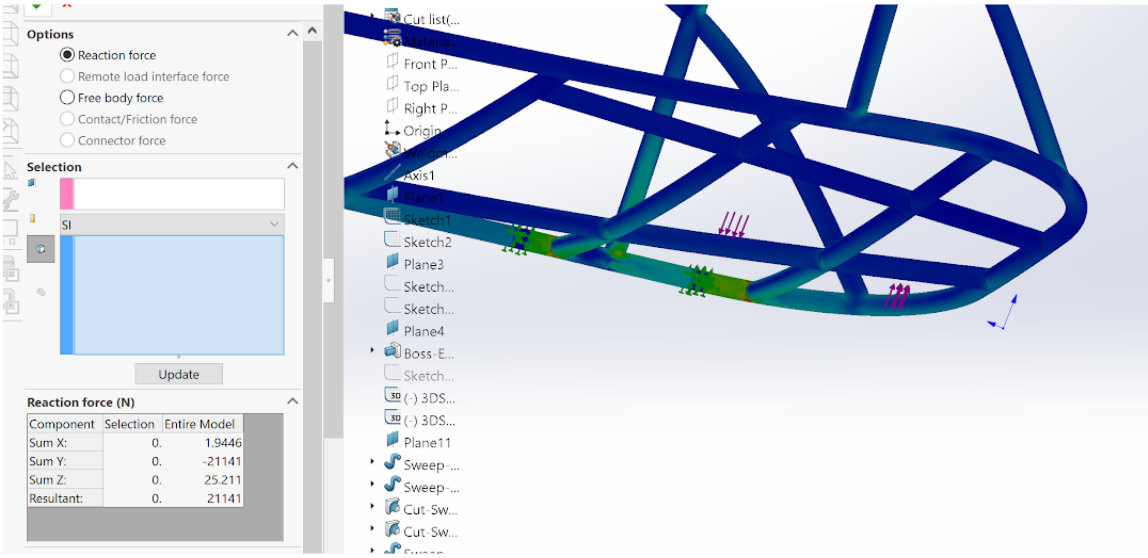

Figure 19. Listing of reaction forces in Solidworks.

Displacement and Mode shape plots

During static and frequency studies, displacement and mode shape animations were referenced. From such visualizations, one can make an intuitive judgment about the accuracy of study based on how realistic the motion appears to be.

4 Discussion

4.1 Boundary Conditions

A fundamental step in FEA process, is when a real structure and loading scenario are turned into a mathematical model. While essential, it also introduces modelling error. This is especially apparent when defining the nodal displacement vector or boundary conditions of a static study model – the $\{D\}$ in the FEA equilibrium equation.

In this particular instance, two sets of boundary conditions are defined for the analysis of the PAL-V chassis. It is felt they do not accurate reflect reality.

In Loading Case 1, the bearings opposite to the touchdown wheel are fixed. This over simplifies the highly unconstrained landing of helicopter, to the loading of a cantilevered beam. While this may capture the “essence of the loading”, it introduces highly unnatural stress behaviour, as seen in Figure 20.

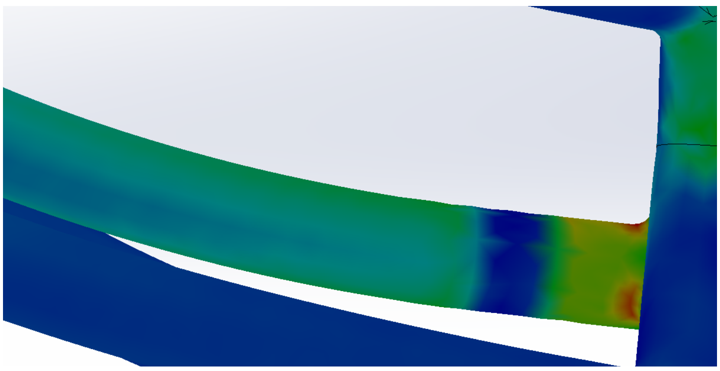

Figure 20. “Stress discontinuity” at bearing boundary location.

In Loading Case 2, the specified boundary condition was to fix the base of the chassis. Suggesting a different interpretation, it was felt that fixing the entire bottom would add redundant supports, and unnecessary stiffness to the model.

Thus only points at which the chassis touches the bearings and front wheel support are fixed. Even so, these fixtures are misplaced. A helicopter in flight is completely unconstrained. In the vibration studies, identical boundary donations were used for consistency with the scenario in Loading Case 2. This was potentially the wrong approach. Other fixture methods were researched, such as using inertia relief, however, ultimately it is felt that the presented static studies are not suitable for this analysis. The results should be taken cautiously.

4.2 Static Studies

Static analysis for 5 separate loading cases has been presented in this paper. In each case, a von Mises criteria was used. Based on the elastic energy of distortion, this criteria predicts failure at $\sigma_v > S_y$, and is used for ductile materials [2]. Subsequently, it is suitable for metals such as aluminum and magnesium alloy.

More illustrative of the static studies, are the mesh convergence plots. Another discrepancy between predictions of a model and real structures is caused by discretization error. This error is clearly evident in these plots.

It should be noted in Figure 12, that by simply reducing maximum element size from 39.4 mm to 3 mm, maximal stress decreased from 174.6 MPa to 100 MPa. Theses error however, are exactly those which mesh convergence tries to eliminate. In general, the finer the mesh, the more accurate the result. One reason for this, is that smaller elements can better approximate irregular shapes and are are less likely to have large aspect ratios. The closer an element aspect ratio is to the ideal element, the more accurate the integral approximations over the element's volume are.

More concerning, are the convergence plots such as Figure 4. As maximum element size from 32.9 mm to 4.6 mm, maximal stress exponentially increases from 819.3 MPa to 968.8 MPa. This indicates a stress singularity, a point in a model who's stress tends towards an infinite value. It is felt that these singularities existed because the chassis structural connections were poorly modelled.

It can be very hard to determine the actually validity of a design, when a stress singularity artificially inflates the maximal stress. Upon reflection the design process, its seems that in the quest to reduce stress caused by mathematical improbabilities, the final structure is one that meets none of the requirements.

4.3 Fatigue Analysis

The Fatigue Analysis conducted on the chassis utilized multiple loads. Rather then test each moment load in isolation, combining them into a single alternating stress better reflects the actually loading scenario. This integration was accomplished using the Solidwork's Find Peaks loading type. Find Peaks functions by calculating the stress values for all possible combinations of stress peaks and then determining which combination produces the largest stress fluctuation. The alternating stress, mean stress and stress ratio can then be calculated from the extremes of the fluctuation.

$$S_{\textbf{alternating}} = \frac{\sigma_{max} - \sigma_{min}}{2} \qquad S_{\textbf{mean}} = \frac{\sigma_{max} + \sigma_{min}}{2} \qquad R = \frac{\sigma_{min}}{\sigma_{max}}$$

Importantly, these values can then be used to calculated a S-N curve correction. Because R is unlikely to be -1, the value for which most S-N curves are derived, a Gerber method should be employed [2].

4.4 Frequency Analysis

The natural frequency of one a dof, 2nd order system is given by

$$\omega = \sqrt{\frac{k}{m}}$$

While in a chassis, there are technically infinite natural frequencies, only the lowest frequency is of concern. More over, it can be analyzed by the same equation. This means that by increasing the stiffness of the structure with minimal additional mass, the natural frequency will increase. This principle provides guidance to increasing the chassis's natural frequency and lends it self naturally to the application of triangles. Hence, the rotor hub was reinforced with a triangular arc was crossed braced with further triangular supports (refer to Figure 1).

4.5 Concluding Remarks

Many times throughout this project, it was forgotten that finite element analysis is tool. Looking back, the questionable decisions made have been a result of trying decrease the FEA stress at the expense of our own mechanics knowledge and physical intuition. Never the less, tool such as FEA, will be invaluable in the future. When used properly, it can enable a design engineer to create complex, yet robust engineered product at a significantly lower cost.

References

[1] PAL-V. (2018). *Explore PAL-V | PAL-V*. [online] Available at: https://www.pal-v.com/en/explore-pal-v [Accessed 22 Mar. 2018].

[2] Ghajari, Mazdak. Finite Element Analysis. Vol. 1.0.

Appendix A

Calculations for forces at bearings. Lengths of structural members are taken from PAL-V assembly file.

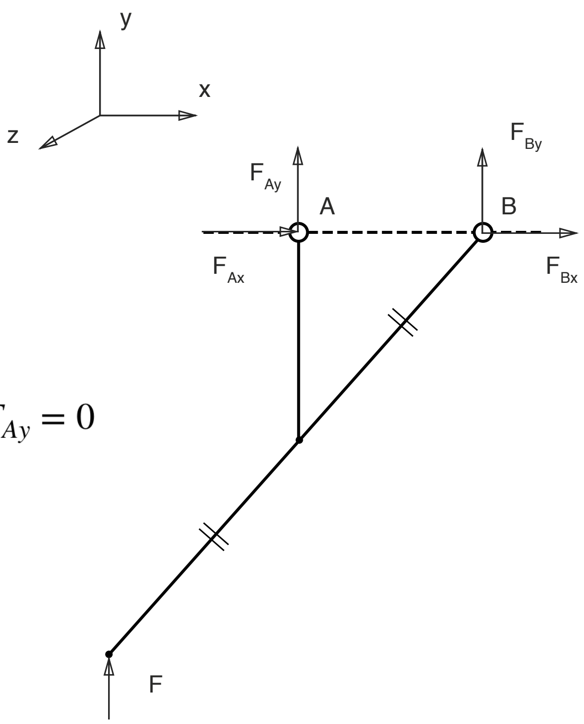

1. $\sum F_x = F_{Ax} + F_{Bx} = 0$
2. $\sum F_y = F + F_{Ay} + F_{By} = 0$
3. $\sum M_B = -\,0.87F + 0.0076F_{Ax} - 0.43F_{Ay} = 0$
4. $\tan\theta = \dfrac{F_{Ax}}{F_{Ay}}$

$\theta \approx 0 \qquad \tan\theta \approx 0 \qquad F_{Bx} \approx 0$

$$\sum F_x = F_{Ax} \approx 0$$

$$\sum M_B = -\,0.87F - 0.43F_{Ay} = 0$$

$$F_{Ay} = \frac{-0.87(7000)}{0.43} = -\,14162.7\ \mathbf{N}$$

$$\sum F_y = 7000 - 14167.7 + F_{By} = 0$$

$$F_{By} = 7162.8\ \mathbf{N}$$

Appendix B

Table 1. C*onvergence Data, Loading Case 1*

Min. Element Size (mm)	Max. Element Size (mm)	Stress (MPa)
7.65	32.98	819.3
5.6	18.6	844.8
4.45	11.13	871
4	7.5	904.4
3.27	4.67	968.8

Table 2. C*onvergence Data, Loading Case 2 – Direction 1*

Min. Element Size (mm)	Max. Element Size (mm)	Stress (MPa)
10.5	65.9	179.7
8	30	181.3
7	25	186.4
6	20	191
5	15	195.6
4	7	210
3	5	209.4

Table 3. C*onvergence Data, Loading Case 2 – Direction 2*

Min. Element Size (mm)	Max. Element Size (mm)	Stress (MPa)
10.5	65.9	176
6.7	20	186.6
4.705	15.6	183.3
3.4	10	203
2	5	250

Table 4. C*onvergence Data, Loading Case 2 – Direction 3*

Min. Element Size (mm)	Max. Element Size (mm)	Stress (MPa)
21.7	108.5	165.5
10.9	65.9	80.6
5	30	91
3	15	94.6
1.5	5	102

Table 5. C*onvergence Data, Loading Case 2 – Direction 4*

Min. Element Size (mm)	Max. Element Size (mm)	Stress (MPa)
20.4	102.2	246.3
7.8	39.4	174.6
4.7	23.6	91.7
3.4	15	94.2
2	10	97
1.5	3	100